JCTC Journal of Chemical Theory and Computation

Article

pubs.acs.org/JCTC

Nucleic Acid Quadruplexes Based on 8-Halo-9-deazaxanthines: Energetics and Noncovalent Interactions in Quadruplex Stems

Yevgen P. Yurenko,[†] Jan Novotný,[†,‡] Mariusz P. Mitoraj,[∥] Vladimir Sklenář,[†,‡,§] Artur Michalak,[∥] and Radek Marek*[,†,‡,§]

[†]CEITEC − Central European Institute of Technology, Masaryk University, Kamenice 5/A4, CZ − 62500 Brno, Czech Republic
[‡]National Center for Biomolecular Research, Faculty of Science, Masaryk University, Kamenice 5, 625 00 Brno, Czech Republic
[∥]Department of Theoretical Chemistry, Faculty of Chemistry, Jagiellonian University, R. Ingardena 3, Krakow PL-30060, Poland
[§]Department of Chemistry, Faculty of Science, Masaryk University, Kamenice 5, 625 00 Brno, Czech Republic

Supporting Information

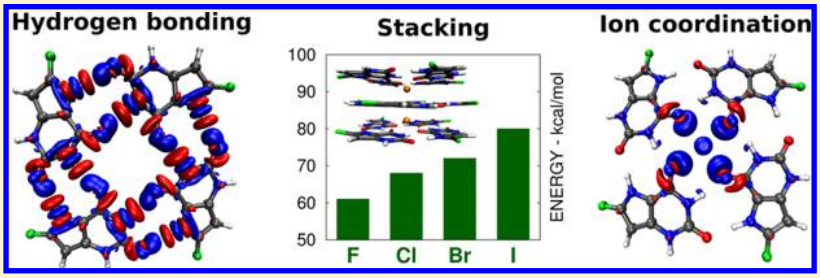

ABSTRACT: Structural and energetic features of artificial DNA quadruplexes consisting of base tetrads and their stacks with Na^+/K^+ ion(s) inside the central pore and incorporating halogenated derivatives of xanthine, 8-fluoro-9-deazaxanthine (FdaX), 8-chloro-9-deazaxanthine (CldaX), 8-bromo-9-deazaxanthine (BrdaX), or 8-iodo-9-deazaxanthine (IdaX), have been investigated by modern state-of-the-art computational tools. The DNA (or RNA) quadruplex models based on 8-halo-9-deazaxanthines are predicted to be more stable relative to those with unmodified xanthine due to the increased stabilizing contributions coming from all three main types of weak interactions (H-bonding, stacking, and ion coordination). Methods for analyzing the electron density are used to understand the nature of forces determining the stability of the system and to gain a predictive potential. Quadruplex systems incorporating polarizable halogen atoms (chlorine, bromine, or iodine) benefit significantly from the stabilizing stacking between the individual tetrads due to an increased dispersion contribution as compared to xanthine and guanine, natural references used. Ion coordination induces a significant rearrangement of electron density in the quadruplex stem as visualized by electron deformation density (EDD) and analyzed by ETS-NOCV and Voronoi charges. Na^+ induces larger electron polarization from the quadruplex toward the ion, whereas K^+ has a higher propensity to electron sharing (identified by QTAIM delocalization index). We expect that our results will contribute to the development of novel strategies to further modify and analyze the natural G-quadruplex core.

1. INTRODUCTION

It is now widely recognized that DNA is a highly adaptable molecule, which determines, to a great extent, the variety of roles it plays in a living cell.[1] Among the possible DNA structural arrangements, G-quadruplexes have gained substantial attention due to their paramount role in a living cell. G-quadruplexes are formed in telomeres at the ends of linear chromosomes.[2] These elements protect the terminal DNA sequences, and their shortening induces the replicative senescence. However, in a cancer cell, the telomerase enzyme maintains the length of telomeres. In this regard, the G-quadruplex is a target for cancer and also antiaging therapy.[3] Besides the role in functioning of telomeres, G-quadruplexes are crucial elements in gene promoters and, therefore, play an important role in expression of genetic material.[4] In addition, several proteins specifically bind to G-quadruplex or perform selective enzymatic activity on G-quadruplex substrates.[5−7] It is noteworthy that only recently G-quadruplexes were directly visualized *in vivo* with the help of an engineered antibody that binds directly to G-tetraplex sites in human chromosomes.[8]

The spatial structure of G-quadruplexes governed by noncovalent interactions[9] can be dissected into three basic organization levels: a) Assembling of four guanine units into the guanine tetrad (G-tetrad or G-quartet) via hydrogen bonds; b) Formation of higher-order assemblies $(G4)_n$ through $\pi-\pi$ stacking interactions of neighboring G-tetrads; c) Coordination of monovalent ions (Na^+, K^+), which are typically located in the interbase regions of the quadruplex channel and impart an additional stability to the quadruplex structure.

Previously, several theoretical approaches were applied to study structure and energetics of nucleic acid quadruplexes,

Received: August 21, 2014
Published: October 21, 2014

   dx.doi.org/10.1021/ct5007554 | *J. Chem. Theory Comput.* 2014, 10, 5353−5365

including those based on *ab initio* quantum chemical calculations[10−25] as well as regular and adaptive biasing force molecular dynamics simulations (refs 26−30 and references therein). In some of them, the nature and strength of H-bonding and ion-base coordination interactions were analyzed.[10−12] Other investigations provided valuable insights into the ion transport in quadruplex channels,[28] nature of quadruplex-ligand interactions,[29] influence of sequence and loop connectivity on G-quadruplex folding,[30] and influence of glycosidic conformational patterns on the energetics of stacking.[19,27] The different simulation approaches and their applicability for exploring structure and dynamics of nucleic acids, including G-DNA and G-RNA, have been recently reviewed by Šponer and co-workers.[27] Despite recent advances, the basic stabilizing factors and structural polymorphism of nucleic acid quadruplexes are still incompletely understood and present a challenge for molecular modeling studies.

A self-assembly of G-quadruplexes[31] is ideal for constructing nanoscale devices[32] due to the unique properties of these systems. G-quadruplexes were shown to be more conductive than double-helical DNA, because they have more π-contacts along the stack as compared with double-stranded DNA.[33] Therefore, the G-tetrad motif can serve as a building block of molecular G-wires,[34] frayed wires,[35] and synapsable quadruplex-mediated fibers[36] and can be useful for developing nanomaterials, mechanical devices, templates, and biosensors.[37] G-quadruplexes can be also employed as artificial ion-transporting transmembrane channels[38] since ions move in the channel of G-quadruplex without disrupting G-tetrads.[39]

In recent years a substantial interest has arisen in modified DNA quadruplexes, due to their potential applications in material science and nanotechnology. The motivation for designing artificial DNA quadruplex structures lies in the fact that in some cases specific properties of G-quadruplexes like conductivity or ability to form particular supramolecular structures should be enhanced. This can be achieved through chemical modifications of nucleobase or/and the sugar−phosphate backbone. It is a matter of fact that base modification may result in substantial distortion of guanine tetrad structure and even in its disruption.[31] For instance, isoguanine (isoG) is prone to form isoG-pentamers in the presence of monovalent ions rather than tetrads.[40] It is notable that some chemical modifications in DNA quadruplexes that impose conformational constraints make them stable even in the absence of ions.[31] Several types of modified DNA quadruplexes have been suggested to act as ditopic ion-pair receptors, i.e. simultaneously coordinate a cation and anion, and serve, among other things, as salt extractors.[41]

Recently, xanthine (X) and its 3-substituted derivatives have been proposed as promising building blocks forming the tetrad structures.[42,43] It was shown that 3-substituted X has a high tendency for self-assembly in the solid state as well as at the solid−liquid interface.[44] For instance, the formation of 3-methylxanthine tetramer and octamer assemblies was experimentally detected by using mass spectrometry and NMR spectroscopy, and their stabilities were confirmed by quantum chemical calculations.[43] The idea of xanthine scaffold for construction of artificial DNA quadruplexes was extended in our recent work.[45] The results of molecular dynamics simulations and adaptive biasing force analysis[45] indicated a high degree of stability of N3-xanthosine-modified DNA quadruplexes and imply a good structural compatibility between artificial tetraplex structures and natural G-quadruplexes. As a next step, we performed a comprehensive analysis of the structure and internal energetics of guanine- and xanthine-based model DNA quadruplexes using high-level quantum chemical calculations.[46] It was shown that whereas G structures benefit from a high degree of H-bond cooperativity,[13] X models are characterized by more favorable and weakly cooperative $\pi-\pi$ stacking.[46] In our latest work,[47] we developed a new *in silico* approach for designing artificial building blocks for DNA quadruplexes derived from the X base. The results of *ab initio* calculations and molecular dynamics simulations suggested[47] 8-halo-9-deazaxanthine base (where halogen is fluorine or chlorine) as a highly promising candidate for developing the artificial quadruplexes and quadruplex-active ligands. In particular, 8-halo-9-deazaxanthine systems are predicted to form quadruplexes with increased stacking stability as compared to the xanthine system and higher affinity toward Na^+ and K^+ ions and approaching the evolution-selected energetic properties of natural guanine system in forming the quadruhelical structure.[47]

In this work, we perform a comprehensive investigation of energetic and structural properties of model DNA quadruplexes containing 8-halo-9-deazaxanthine systems (first described in ref 47). Using high-level modern theoretical approaches (DFT-D calculations, Quantum Theory of Atoms in Molecules,[48] Natural Bond Orbital analysis,[49] Compliance Constant Theory,[50−54] Energy Decomposition analysis[55,56] combined with ETS-NOCV approach,[57,58] and Non-Covalent Interaction (NCI) plots[59,60]), we aim at elucidating the fundamental noncovalent interactions responsible for shaping these structures as well as describing their relative impact on the stability and the molecular geometry. We also characterize individual hydrogen bonds, van der Waals contacts, and metal-base coordination bonds and their mutual influence. This study outlines a comprehensive computational strategy applicable for designing and analyzing new artificial DNA quadruplexes containing modified nucleobases.[61]

2. COMPUTATIONAL METHODOLOGY

Structure and Bonding. In this work, we used the following models representing artificial DNA quadruplexes with 8-halo-9-deazaxanthines: H-bonded base tetrads B4 [where base B is 8-fluoro-9-deazaxanthine (abbreviated as FdaX), 8-chloro-9-deazaxanthine (CldaX), 8-bromo-9-deazaxanthine (BrdaX), or 8-iodo-9-deazaxanthine (IdaX)], base tetrads with coordinated monovalent ion M^+, $B4{\cdot}M^+$ ($M^+ = Na^+, K^+$, Figure 1), two H-bonded tetrads stacked on each other, i.e. $(B4)_2$, two stacked tetrads containing a metal ion located in interplane region, $(B4)_2{\cdot}M^+$, three tetrads stacked on each other without metal ions inside the cavity, $(B4)_3$, as well as three stacked tetrads with one or two metal ions inside the channel denoted as $(B4)_3{\cdot}1M^+$ and $(B4)_3{\cdot}2M^+$, respectively (Figure 2, Figures S1 and S2 in the Supporting Information). Hereafter the general notation for all one-, two-, and three-tetrad models will be B4, $(B4)_2$, and $(B4)_3$, respectively.

The molecular geometries of FdaX- and CldaX-containing models obtained at the BLYP-D3/def2-TZVPP level of theory using COSMO[62] model for water (as implemented in TURBOMOLE V. 6.3 program[63]), were taken from our previous work[47] (for more detailed information, see also Computational Details in the Supporting Information). The structures containing BrdaX and IdaX bases were optimized in this work at the BLYP-D3/def2-TZVPP level of theory, for IdaX taking into account the relativistic effects in the framework

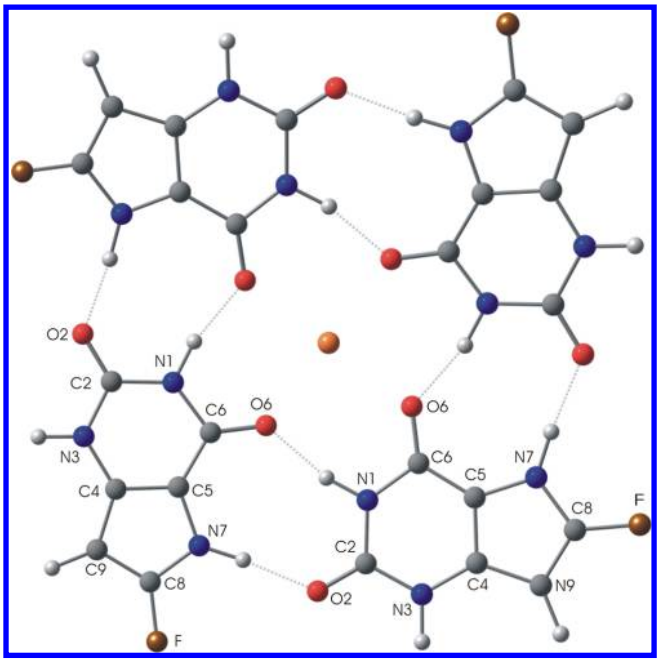

Figure 1. Spatial structure of FdaX quartet with Na^+ cation optimized in the TURBOMOLE program at the BLYP-D3/def2-TZVPP level of theory using the COSMO model for water. The atom numbering corresponds to standard nucleic acid nomenclature.[1] The dotted lines denote hydrogen bonds.

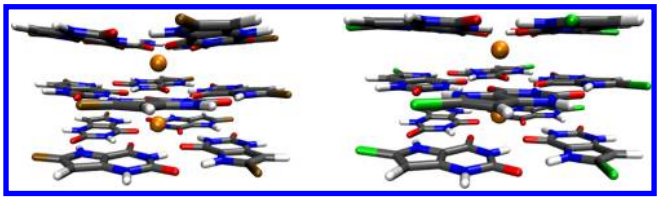

Figure 2. Optimized geometries of $(FdaX4)_3{\cdot}2Na^+$ (left) and $(CldaX4)_3{\cdot}2Na^+$ (right) three-stack systems obtained at the BLYP-D3/def2-TZVPP level of theory in TURBOMOLE using the COSMO model for water.

of effective core potentials (ECP).[63] The use of BLYP[64,65] functional in combination with the recent D3 Grimme's empirical dispersion correction[66] is justified by the fact that BLYP-D method earlier demonstrated an excellent performance for systems of stacked nucleobase pairs and quartets[41] (in particular, calculated stacking energies[41] were in a perfect agreement with the with MP2 and CCSD(T) complete basis set limit energies from the S22 benchmark database[67]). It was earlier shown that empirical dispersion correction does not need to be modified in case of continuum solvation models.[68]

The formation energy of complexes was calculated as the difference between energy of optimized complex and corresponding components optimized at the same level of theory, i.e.

$$\Delta E_{form}[AB] = E[AB] - (E[A] + E[B]) \quad (1)$$

Basis set superposition error (BSSE) was not taken into account since empirical dispersion potential is able to absorb small BSSE effects.[13]

Energy Decomposition Analysis (EDA) and ETS-NOCV. To elucidate the physical nature of noncovalent interactions, which govern the 8-halo-9-deazaxanthine-containing model DNA quadruplex structures, we resorted to the energy decomposition analysis (EDA)[55,56] as implemented in the ADF program.[69] EDA calculations were carried out at the BLYP-D3/TZP level of theory (including ZORA approach for BrdaX and IdaX) for TURBOMOLE geometries[47] obtained at the BLYP-D3/def2-TZVPP level of theory. To check whether EDA results depend on the level of theory/software package in which the geometries were optimized, the B4 and $(B4)_2$ models were also reoptimized at the BLYP-D3/TZP level of theory in the ADF program and afterward were subject to EDA at the same theory level. EDA allows splitting the interaction energy ΔE_{int} between arbitrarily selected molecular regions into four physically meaningful components: classical electrostatic interaction, ΔV_{elstat}, between fragments as they are brought to their positions in the final complex, exchange-repulsion term, ΔE_{ex}, orbital interaction term, ΔE_{oi}, (accounting for charge transfer from one region to other region(s) as well as for polarization within one region), and dispersion energy term, ΔE_{disp}:

$$\Delta E_{int} = \Delta V_{elstat} + \Delta E_{ex} + \Delta E_{oi} + \Delta E_{disp} \quad (2)$$

The molecular regions for EDA were selected in such a way that allows approximate separating and evaluating contribution of a particular type of noncovalent interaction (H-bonding, $\pi-\pi$ stacking, and ion coordination) to the internal stability of B4, $(B4)_2$, and $(B4)_3$ complexes.

To provide insights into directions of charge flow upon formation of noncovalent interactions in the studied DNA quadruplex models, we used the ETS-NOCV approach as implemented in the ADF package.[69] This approach represents combination of the extended transition state (ETS)[70] with natural orbitals for chemical valence (NOCV) scheme.[57,58] NOCVs have been derived[71] as eigenvectors that diagonalize the electron deformation density matrix.[57] It was shown[57] that the NOCV pairs (Ψ_{-k}, Ψ_k) decompose the differential density $\Delta\rho$ into NOCV contributions $(\Delta\rho_k)$

$$\Delta\rho(r) = \sum_{k=1}^{M/2} \nu_k[-\Psi^2_{-k}(r) + \Psi^2_k(r)] = \sum_{k=1}^{M/2} \Delta\rho_k(r) \quad (3)$$

where ν_k denotes NOCV eigenvalues, M stands for the number of basis functions, and k marks a number of a contribution from a particular NOCV pair. The ETS-NOCV[57] scheme makes it possible to decompose the orbital interaction term ΔE_{oi} from eq 2 into the contributions corresponding to NOCV charge-transfer channels, $\Delta\rho_k$; E^k_{orb}:

$$\Delta E_{orb} = \sum_k \Delta E^k_{orb} \quad (4)$$

The above components E^k_{orb} provide energetic estimation of $\Delta\rho_k$ that may be related to the importance of a particular electron flow channel for the bonding between considered molecular fragments.

Quantum Theory of Atoms in Molecules (QTAIM). Noncovalent interactions (H-bonds, van der Waals contacts, and ion-base coordination contacts) in model quadruplex structures were initially indicated using the QTAIM approach[48] implemented in the AIMAll program.[72] The presence of a (3,−1) critical point, alternatively called a line critical point[73] (LCP), and a line path between two atoms as well as a positive value of the electron density Laplacian, $\nabla^2\rho$, were considered as possible indicators of formation of a closed-shell interaction (H-bond, van der Waals contact, or ion-base coordination bond). The wave functions for QTAIM analysis were computed

dx.doi.org/10.1021/ct5007554 | J. Chem. Theory Comput. 2014, 10, 5353−5365

in the Gaussian 09 suite of programs[74] at the BLYP/def2-TZVPP level of theory for TURBOMOLE geometries (the def2-TZVPP[75] basis set was imported from the EMSL Basis Set Library).[76,77] The charge transfer properties of H-bonds were additionally studied by NBO analysis[49] (see the Computational Details section in the Supporting Information).

The H-bond energies were evaluated by several independent methods. The first one is the Espinosa−Molins−Lecomte approach[78] based on topological characteristics at LCPs (3,−1) of H-bonds

$$E_{HB} = 0.5V(r) \quad (5)$$

where $V(r)$ is the value of a local potential energy density (virial field) at the (3,−1) CPs. Since formula 5 is reported[79] to overestimate H-bond energy, we also used an alternative formula suggested by Nikolaienko et al.:[80] $E_{NH\cdots O}$ [kcal/mol] = $-2.03 + 225\cdot\rho^{LCP}$, where ρ^{LCP} is the electron density at LCP (in atomic units). This formula was derived by comparing QTAIM and vibrational characteristics (such as frequency red shifts for stretching vibrations) for a large number of NH···O hydrogen bonds in DNA-related biomolecules.[80] In addition, the Delocalization Index (DI) as defined in the QTAIM was used to characterize the covalency of individual intermolecular bonds.[48,73]

Compliance Constants and Non-Covalent Interaction (NCI) Analysis. The relative strengths of H-bonds, metal-base coordination bonds, and van der Waals contacts were additionally evaluated by means of the compliance constants formalism,[50−52] which was shown to be suitable for analysis of intermolecular[81] and intramolecular[82,83] H-bonds in DNA constituents (see the Computational Details section in the Supporting Information).

Finally, the locations of noncovalent interactions were visualized by Non-Covalent Interaction (NCI) plot analysis[59,60] based on the relationship between the reduced electron density gradient $s(r)$ and $sign(\lambda_2)\rho$, where λ_2 is the second eigenvalue of the electron density Hessian, and ρ is the electron density. This method also allows distinguishing between different types of weak interactions by analyzing contributions to the electron density Laplacian $\nabla^2\rho$ along the axes of its maximal variation. These contributions are the eigenvalues λ_i of the electron-density Hessian (second derivative) matrix, such that $\nabla^2\rho = \lambda_1 + \lambda_2 + \lambda_3$. For H-bonds the second eigenvalue (λ_2) is negative, since they are characterized by accumulation of density perpendicular to the bond. On the other hand, van der Waals contacts are characterized by a negligible density overlap that gives $\lambda_{2\approx} < 0$. The NCI analysis was performed in the NCIPLOT[60] program using promolecular electron densities.

3. RESULTS AND DISCUSSION

3.1. Energetic Characteristics and Structural Properties of Model DNA Quadruplex Structures. It has been demonstrated[13,43,45,46] that the xanthine (X) base satisfies steric and electronic requirements for compatibility with the natural G base and can be considered as a promising candidate for construction of artificial DNA quadruplexes. Recently, we have developed a novel strategy of xanthine core modifications yielding DNA quadruplexes, which benefit from an even higher degree of stability of modified systems.[47] This strategy allowed us to identify, among many other possible modifications of xanthine, two 8-halo-9-deazaxanthine derivatives − 8-fluoro-9-deazaxanthine (FdaX) and 8-chloro-9-deazaxanthine (CldaX) − as the most perspective structural elements for building artificial DNA quadruplex structures.[47] The proposed X-core modifications should yield structures, which would be sterically compatible (for calculated molecular volumes, see Table S1 in the Supporting Information)[84] with naturally occurring stacks of G-tetrads.

Merz−Singh−Kollman (ESP) charges on atoms in FdaX and CldaX monomeric units involved in H-bonding (Table 1) represent a simple way to roughly estimate the tendency for the base self-association via hydrogen bonds. In addition to previously designed FdaX and CldaX, we also analyzed partial charges in two other 8-halo-9-deazaxanthine monomers containing more polarizable halogen atoms, specifically 8-bromo-9-deazaxanthine (BrdaX) and 8-iodo-9-deazaxanthine (IdaX). Based on this analysis, the following observations can be made: (i) The O6 atom in FdaX, CldaX, and BrdaX derivatives bears a more negative partial charge as compared to the unmodified xanthine (X)[46] (Table 1). In contrast, in the IdaX derivative the O6 charge is slightly more positive relative to X. It may therefore be assumed that a metal cation coordination to O6 atom as well as the strength of the internal N1H···O6 hydrogen bond should be enhanced in FdaX, CldaX, and BrdaX relative to X; (ii) The O2 atom in all 8-halo-9-deazaxanthine units is characterized by slightly higher negative charge relative to unmodified X,[46] which makes it a better acceptor for the N7H···O2 hydrogen bond; (iii) On the contrary, H1 and H7 atoms in 8-halo-9-deazaxanthines, which can be involved in N1H···O6 and N7H···O2 hydrogen bonds, respectively, are slightly less positively charged than those in X, which indicates a lower polarity of hydrogen-bond donating N1H and N7H groups in these systems.

Table 1. ESP-Kolmann Atomic Charges Calculated for FdaX, CldaX, BrdaX, and IdaX Monomeric Units[a]

	O6	H1	O2	H7/N7	NH2
FdaX	−0.644	0.374	−0.667	0.392	
CldaX	−0.626	0.368	−0.668	0.330	
BrdaX	−0.621	0.365	−0.670	0.309	
IdaX	−0.616	0.360	−0.672	0.276	
X	−0.620	0.404	−0.663	0.404	
G	−0.639	0.415		−0.703	0.402/0.406

[a]For reference purposes, the atomic charges for xanthine (X) and guanine (G), reported earlier,[46] are also listed.

Energetics is one of the crucial factors that drive the molecular self-assembly. First, we analyzed the formation energies in solution (using the COSMO[62] model for water) for the tetrads B4 as well as for the two-stack $(B4)_2$ and three-stack $(B4)_3$ systems (Table S2 in the Supporting Information). In our previous work[46] we have shown that xanthine-based model DNA quadruplex structures are characterized by more favorable $\pi-\pi$ stacking than the corresponding G-containing models. Since base stacking in nucleic acids is described by three main contributions, namely, electrostatic interaction, London dispersion attraction, and short-range repulsion,[85] we expected that the presence of halogen atoms near the C8 atom and increase of the system size (8-halo-9-deazaX base contains 16 atoms vs 15 atoms in X) will reinforce the electrostatic and dispersion terms due to enhancement of dipole−dipole interaction and the number of available electrons in the system, respectively. Indeed, the formation of two-stack systems $(FdaX4)_2$ and $(CldaX4)_2$ from two isolated tetrads FdaX4 and CldaX4 yields the energy gain of −31 kcal/mol and −35

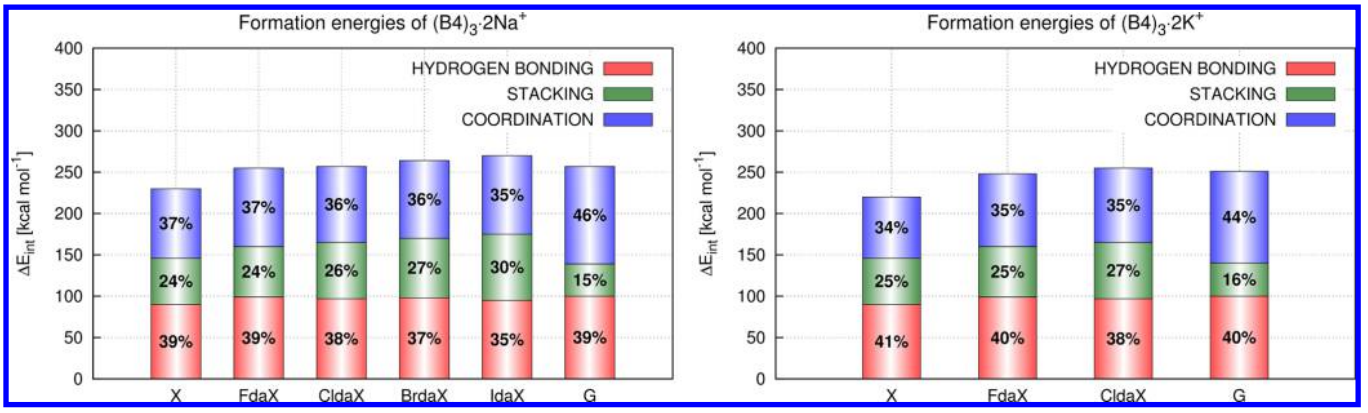

Figure 3. Relative contributions (in %) of H-bonding, aromatic $\pi-\pi$ stacking, and Na^+/K^+ coordination to the formation energies ΔE_{form} (eq 1 in Computational Methodology) in three-stack $(B4)_3 \cdot 2Na^+$ (left) and $(B4)_3 \cdot 2K^+$ (right) complexes of 8-halo-9-deazaxanthine derivatives (FdaX, CldaX, BrdaX, and IdaX) as compared to X and G from our previous work.[46] The geometries were optimized in TURBOMOLE at the BLYP-D3/def2-TZVPP level of theory using COSMO model for water. Contributions (in %) of noncovalent interactions were estimated by means of the following formulas: H-bonding contribution = $\{n^*(E[B4]-4^*E[B])\}/\Delta E_{form}$, where E[B4] – electronic energies of individual tetrads in two- and three-stack systems, E[B] – energies of isolated bases; Stacking contribution = $(E[(B4)_n]-n^*E[B4])/\Delta E_{form}$; Ion coordination contribution = $\{E[(B4)_n \cdot (n-1)M^+]-[E(B4)_n]-(n\text{-}1)^*E[M^+]\}/\Delta E_{form}$, where n = 3 for $(B4)_3 \cdot 2M^+$ models.

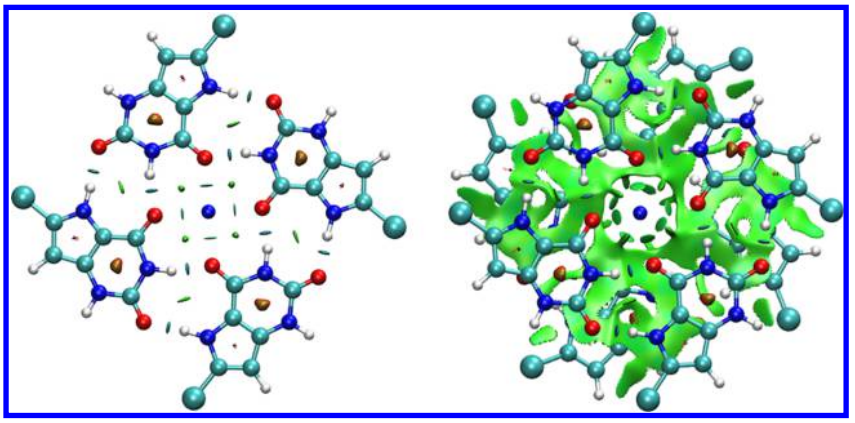

Figure 4. NCI surfaces of the $CldaX4 \cdot Na^+$ (left) and $(CldaX4)_2 \cdot Na^+$ (right) complexes. The NCI analysis was carried out employing promolecular densities. The cutoff for the reduced density gradient is 0.4 au. The NCI surfaces for corresponding structures with xanthine (X) and FdaX are presented in Figure S3 in the Supporting Information.

kcal/mol, respectively, which clearly exceeds the corresponding values for $(X4)_2$ and $(G4)_2$ complexes (−27 kcal/mol and −22 kcal/mol, Table S2 in the Supporting Information). It should be also noted that the above-mentioned strengthening is more pronounced in systems containing more polarizable halogen atom. The analysis of formation energies indicates that in the model DNA quadruplex structures based on 8-halo-9-deaza derivatives of xanthine all three main types of noncovalent interactions – H-bonding, $\pi-\pi$ stacking, and ion coordination are enhanced relative to X-containing quadruplexes (Figure 3).

Since H-bonding, stacking, and cation coordination inside the central pore represent three major noncovalent forces governing various arrangements of DNA quadruplex stems, it is crucial to evaluate their relative contributions to the stability. The obtained data suggest that in the case of F- and Cl-containing DNA quadruplex models,[46] hydrogen bonding and ion coordination generate the greatest contribution (~35–40%) to the stability of $(B4)_3 \cdot 2M^+$ complexes, whereas all three terms (hydrogen bonding, aromatic $\pi-\pi$ stacking, and ion coordination) become almost equally important for the polarizable IdaX system (Figure 3). For complexes with unmodified X and its halogen derivatives the contribution of the stacking increases by 10–15% relative to that for $(G4)_2 \cdot 2M^+$ models.

As far as structural properties of model DNA quadruplexes are concerned, it should be noted that in our model complexes the individual tetrads manifest some deviation from planarity (Table S3 and Table S4 and related comments in the Supporting Information). The analysis of RMSD values shows that the most substantial degree of nonplanarity is observed in the case of tetrad models B4, whereas in higher-order $(B4)_2$ and $(B4)_3$ complexes the parallel stacked layers are found to be more planar. This can be explained by the fact that more planar arrangement of tetrads in $(B4)_2$ and $(B4)_3$ systems enhances the $\pi-\pi$ stacking interactions. In addition, Na^+/K^+ coordination with carbonyl groups effectively compensates for the repulsion between the negatively charged O6 atoms of the stacked tetrads and thus also promotes the tetrad planarity.

3.2. General Overview of Noncovalent Interactions in 8-Halo-9-deazaxanthine-Based Model Quadruplexes.

Non-Covalent Interaction (NCI) Plots. As mentioned above, the H-bonding, aromatic $\pi-\pi$ stacking, and metal ion coordination represent three major noncovalent forces that determine spatial structures of quadruplexes and their properties. Non-Covalent Interaction (NCI)[59,60] plot analysis enables

dx.doi.org/10.1021/ct5007554 | J. Chem. Theory Comput. 2014, 10, 5353–5365

Table 2. Energy Decomposition Analysis (EDA) of Interaction Energies, ΔE_{int}, between Different Regions of Model DNA Quadruplexes Containing 8-Halo-9-deazaxanthine Derivatives[d]

base	type of noncovalent interaction	model/optimized structure[a]	ΔE_{oi}	ΔE_{ex}	ΔV_{elstat}	ΔE_{disp}	$\Delta E_{int} = \Sigma\Delta E_i$	VDD[b] (ion)
FdaX	H-bonding	B + B/B_2	−17.95	28.28	−24.70	−4.26	−18.62	
		B2 + B2/B4	−36.40	56.89	−49.35	−8.87	−37.73	
	stacking	B4 + $B4/(B4)_2$	−13.59	63.33	−24.55	−72.56	−47.37	
		B4 + B4 + $B4/(B4)_3$	−27.93	129.17	−49.96	−149.29	−98.02	
	ion coordination	B4 + $Na^+/B4{\cdot}Na^+$	−37.41	21.77	−75.40	−5.66	−96.70	−0.085
		$(B4)_2$ + $Na^+/(B4)_2{\cdot}Na^+$	−39.97	9.59	−83.73	−14.44	−128.54	−0.080
		$(B4)_3$ + $Na^+/(B4)_3{\cdot}1Na^+$	−42.90	11.67	−85.40	−14.82	−131.45	−0.080
		$(B4)_3{\cdot}Na^+$ + $Na^+/(B4)_3{\cdot}2Na^+$	−42.81	13.50	−39.13	−15.10	−83.54	−0.082
		B4 + $K^+/B4{\cdot}K^+$	−26.54	17.99	−55.90	−7.47	−71.92	−0.057
		$(B4)_2$ + $K^+/(B4)_2{\cdot}K^+$	−38.80	26.93	−79.96	−15.36	−107.19	−0.057
		$(B4)_3$ + $K^+/(B4)_3{\cdot}1K^+$	−41.85	28.73	−80.68	−15.37	−109.17	−0.058
		$(B4)_3{\cdot}K^+$ + $K^+/(B4)_3{\cdot}2K^+$	−40.36	30.20	−31.74	−17.10	−59.00	−0.062
CldaX	H-bonding	B + B/B_2	−17.33	27.85	−24.07	−4.53	−18.08	
		B2 + B2/B4	−35.11	55.89	−48.08	−9.34	−36.64	
	stacking	B4 + $B4/(B4)_2$	−15.33	71.03	−26.84	−82.22	−53.37	
		B4 + B4 + $B4/(B4)_3$	−31.86	147.06	−56.39	−169.85	−111.03	
	ion coordination	B4 + $Na^+/B4{\cdot}Na^+$	−38.14	22.68	−76.64	−5.66	−97.75	−0.085
		$(B4)_2$ + $Na^+/(B4)_2{\cdot}Na^+$	−40.15	8.81	−82.60	−14.30	−128.24	−0.080
		$(B4)_3$ + $Na^+/(B4)_3{\cdot}1Na^+$	−42.49	11.23	−87.38	−14.95	−133.60	−0.080
		$(B4)_3{\cdot}Na^+$ + $Na^+/(B4)_3{\cdot}2Na^+$	−43.21	13.44	−39.32	−15.18	−84.27	−0.082
		B4 + $K^+/B4{\cdot}K^+$	−26.68	17.74	−55.51	−7.50	−71.95	−0.057
		$(B4)_2$ + $K^+/(B4)_2{\cdot}K^+$	−39.66	29.31	−82.46	−14.98	−107.79	−0.057
		$(B4)_3$ + $K^+/(B4)_3{\cdot}1K^+$	−40.84	28.17	−83.95	−15.74	−112.36	−0.058
		$(B4)_3{\cdot}K^+$ + $K^+/(B4)_3{\cdot}2K^+$	−40.51	30.20	−32.63	−17.16	−60.10	−0.062
BrdaX[c]	H-bonding	B2 + B2/B4	−35.04	55.99	−47.82	−9.58	−36.45	
	stacking	B4 + B4 + $B4/(B4)_3$	−33.76	152.75	−58.55	−177.99	−117.55	
	ion coordination	$(B4)_3{\cdot}Na^+$ + $Na^+/(B4)_3{\cdot}2Na^+$	−43.70	13.75	−40.47	−15.13	−85.55	−0.082
IdaX[c]	H-bonding	B2 + B2/B4	−34.84	56.05	−47.71	−9.87	−36.37	
	stacking	B4 + B4 + $B4/(B4)_3$	−35.52	160.74	−57.71	−188.29	−120.78	
	ion coordination	$(B4)_3{\cdot}Na^+$ + $Na^+/(B4)_3{\cdot}2Na^+$	−43.79	13.50	−42.38	−15.11	−87.78	−0.082

[a]B + B − formation of Hoogsteen base pair from two bases, B2 + B2 − formation of tetrad from two H-bonded Hoogsteen base pairs, B4 + B4 − formation of a hollow $(B4)_2$ system from two tetrads, B4 + B4+ B4 − interaction of an internal tetrad with two external tetrads in a three-stacked system, B4 + Na^+ and B4 + K^+ − formation of tetrads with a coordinated ion by adding sodium and potassium cations, respectively, $(B4)_2$ + Na^+ and $(B4)_2$ + K^+ − formation of $(B4)_2$ models with a coordinated ion by adding sodium and potassium cations, $(B4)_3$ + Na^+ and $(B4)_3$ + K^+ − interaction of a stacked three-tetrad system with a coordinated Na^+/K^+ cation, $(B4)_3{\cdot}Na^+/K^+$ + Na^+/K^+ − interaction of a stacked three-tetrad system with Na^+/K^+ when the other ion is located inside the channel. [b]Voronoi deformation density of Na^+/K^+ cation in a complex. [c]Calculated by means of ZORA approach using relativistic scalar Hamiltonian.[97] [d]Model regions were chosen in such a way that allows for the separation of approximately contributions of different types of noncovalent interactions. EDA was performed at the BLYP-D3/TZP level of theory for TURBOMOLE geometries (obtained at the BLYP-D3/def2-TZVPP level of theory using COSMO continuum solvent model for water). Energy unit is kcal/mol.

direct visualization of noncovalent interactions and the rough estimation of their strength. Figure 4 displays NCI surfaces for two structures − tetrad CldaX4·Na^+ and two-stack model $(CldaX4)_2{\cdot}Na^+$ (the NCI surfaces for corresponding structures with FdaX and unmodified X[46] bases are shown in Figure S3 in the Supporting Information). The blue ellipsoids appearing between the hydrogens and H-bond acceptors indicate the presence of strong H-bonds. The cation-base coordination contacts are manifested by regions that are located directly between the Na^+ cation and the O6 atoms in each nucleobase unit (Figures 4 and S3, left). $\pi-\pi$ stacking interactions emerge as large green surfaces between planes of parallel tetrads (Figures 4 and S3, right).

The N1H···O6 and N7H···O2 hydrogen bonds in the $(CldaX4)_2{\cdot}Na^+$ and $(FdaX4)_2{\cdot}Na^+$ complexes are displayed as two peaks with $sign(\lambda_2)\rho$ value ∼ −0.05 au at the reduced density gradient plot (Figure S4). It is remarkable that these peaks almost merge indicating similar strengths of N1H···O6 and N7H···O2 hydrogen bonds. For comparison, in the two-stack model of unmodified xanthine, $(X4)_2{\cdot}Na^+$, the $sign(\lambda_2)\rho$ = −0.05 au (Figure S4) for the N1H···O6 interaction as in the $(CldaX4)_2{\cdot}Na^+$ and $(FdaX4)_2{\cdot}Na^+$ complexes but a different one (−0.04 au) is found for the N7H···O2 bond.[46] Thus, NCI plot analysis indicates that comparing to $(X4)_2{\cdot}Na^+$ in both $(FdaX4)_2{\cdot}Na^+$ and $(CldaX4)_2{\cdot}Na^+$ models the external H-bonds N7H···O2 get stronger, whereas the internal ones (N1H···O6) retain more or less of the same strength. Such an increase in the N7H···O2 hydrogen bond strength upon xanthine core modification (resulting in the $sign(\lambda_2)\rho$ change from ∼−0.04 au to ∼−0.05 au) may not seem to be substantial; however, we should bear in mind that every tetrad in quadruplexes contains four hydrogen bonds of the N7H···O2 type, so the total quadruplex stabilization coming from a small enhancement of each H-bond can be substantial taking into account a number of stacking tetrads in quadruplexes. It is noteworthy that the described results perfectly agree with H-bond energies[46] for $(FdaX4)_2{\cdot}Na^+$, $(CldaX4)_2{\cdot}Na^+$, and $(X4)_2{\cdot}Na^+$ (Table 3 and Table S5 in the Supporting Information), calculated using QTAIM-based approaches (*vide infra*). For instance, the average calculated energies of N7H···O2 hydrogen

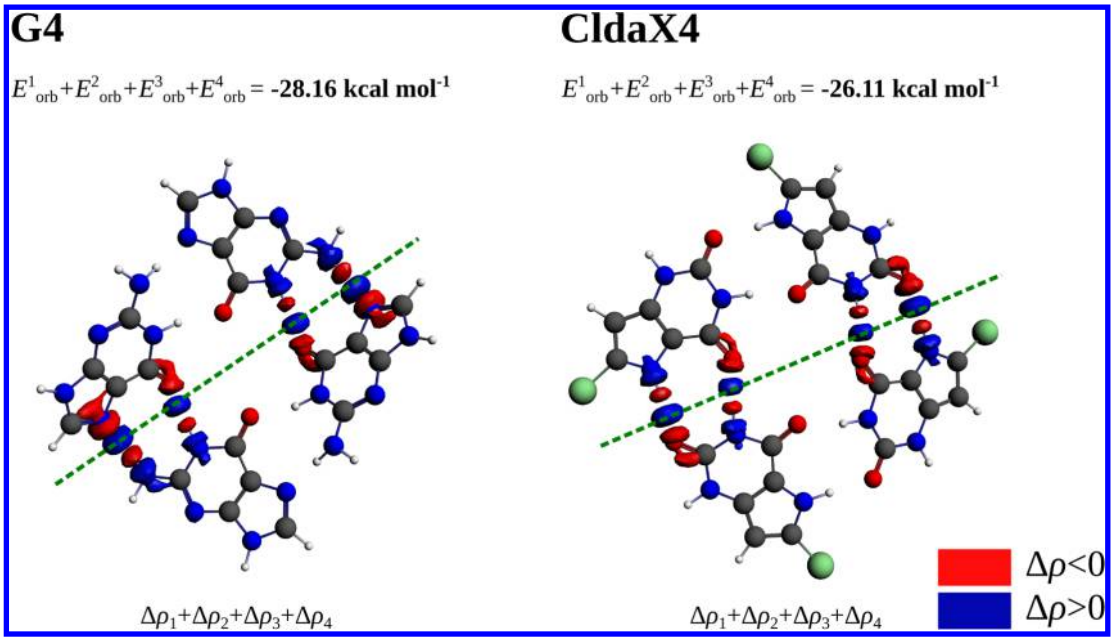

Figure 5. Sums of electron deformation density (EDD) contributions $\Delta\rho_1$, $\Delta\rho_2$, $\Delta\rho_3$, and $\Delta\rho_4$ describing the formation of internal (N1H···O6) and external (N2H···N7/N7H···O2) H-bonds in G4 and CldaX4 tetrads. The contour values are ±0.001 au.

bonds in two-stack systems $(X4)_2{\cdot}Na^+$ and $(CldaX4)_2{\cdot}Na^+$ are 9.15 and 10.74 kcal/mol, respectively. In addition, the calculated NCI green (van der Waals; Figure 4, right) surface areas for $(X4)_2{\cdot}Na^+$, $(FdaX4)_2{\cdot}Na^+$, and $(CldaX4)_2{\cdot}Na^+$ models (see comments to Figure S4 in the Supporting Information) well correlate with stacking energies in corresponding $(B4)_2$ systems (Table 2) and thus demonstrate an increased stabilization coming from the $\pi-\pi$ stacking. In general, NCI plot analysis indicates that the proposed xanthine core modifications lead to stronger H-bonding and stacking contributions in model DNA quadruplexes.

Energy Decomposition Analysis (EDA). To understand the main physical forces that contribute to individual noncovalent interactions in our model systems, we resorted to energy decomposition analysis (EDA)[55,56] implemented in the ADF[69] suite of programs. EDA was performed at the BLYP-D3/TZP level of theory for the BLYP-D3/def2-TZVPP geometries optimized with TURBOMOLE[63] package (Table 2). Contributions of each type of noncovalent forces to stability of model complexes were analyzed by an appropriate selection of the interacting molecular regions (for details, see Table 2 footnotes). The results of EDA point to the following general features of noncovalent interactions in studied systems: (i) In all 8-halo-9-deazaxanthine systems H-bonds are characterized by a prevailing contribution of the electrostatic term, ΔV_{elstat}. However, the orbital interaction term, ΔE_{oi}, plays also an important role covering a large part of the interaction energy and is crucial for balancing the destabilizing exchange-repulsion part. In general, systems with all studied nucleobases (FdaX, CldaX, BrdaX, and IdaX) show similar H-bonding energetics; (ii) Although $\pi-\pi$ stacking is dominated by the dispersion contribution, ΔE_{disp}, the electrostatic term, ΔV_{elstat}, plays an important stabilizing role. The stacking interaction becomes more favorable as the size and polarizability of halogen atom at position 8 increases (i.e., from FdaX to IdaX) and this rise of stacking energy is determined by an augmented contribution of the dispersion term, ΔE_{disp}; (iii) The Na^+ binding to quadruplexes is more stabilizing than K^+ ion, which is due to much higher (positive) exchange-repulsion term, ΔE_{ex}, in the latter case. Overall, Na^+/K^+ interaction gradually becomes more favorable when the halogen atom at position 8 of the base is more polarizable (i.e., from FdaX- to IdaX-containing complexes). This rather small energy gain is controlled by the electrostatic term, ΔV_{elstat}. The next sections describe H-bonding, stacking, and ion coordination in model quadruplex structures in more details.

3.3. Hydrogen Bonding. *Energy Decomposition Analysis.* First, we analyzed the simplest systems − Hoogsteen hydrogen-bonded base pairs FdaX2 and CldaX2 (Table 2). The interaction energy between two bases is ∼−18.5 kcal/mol. The interaction energy associated with the formation of tetrads B4 from two Hoogsteen base pairs B2 corresponds to the formation of two pairs of HBs (−36.6 to −37.7 kcal/mol, Table 2), i.e. the doubled interaction energy between two bases in optimized dimers. The relative proportions of ΔE_{oi}, ΔE_{ex}, ΔV_{elstat}, and ΔE_{disp} terms in the interaction energy, ΔE_{int}, in quartets are similar to those in dimers. In addition to FdaX and CldaX, we explored properties of tetrads incorporating 8-bromo-9-deazaxanthine and 9-deaza-8-iodo-xanthine (hereafter denoted as BrdaX and IdaX, respectively). The results shown in Table 2 provide evidence that interaction energies, ΔE_{int}, between base pairs in BrdaX4 and IdaX4 tetrads and contributions of individual terms to ΔE_{int} are very similar to the above-mentioned data for FdaX4 and CldaX4 complexes. Thus, replacement of F or Cl by heavier halogen atoms Br or I should not affect H-bond characteristics in tetrads.

To sum up, EDA results carried out for the base pairs and tetrads with 8-halo-9-deazaxanthines show that (i) Hydrogen bonding in 8-halo-9-deazaX dimers and quartets is characterized by an important input of the orbital term, ΔE_{oi}, which contributes to counterbalancing the destabilizing exchange-repulsion part; (ii) In contrast to G-quartets,[13] the H-bonds in 8-halo-9-deazaX tetramers show little or no cooperativity. It should be also noted that EDA for geometries optimized using TURBOMOLE and ADF programs (Table 2 and Table S6 in the Supporting Information) yields similar results.

dx.doi.org/10.1021/ct5007554 | J. Chem. Theory Comput. 2014, 10, 5353−5365

Table 3. QTAIM Characteristics of H-Bonds in B4 and $(B4)_2$ Models Containing FdaX and CldaX[g]

structure	H-bond	N^a	ρ^b	$\Delta\rho^b$	$E_{HB}{}^c$	$\sum E_{HB}{}^d$	H^e
FdaX4	N1H···O6	4	0.037	0.098	10.31−10.36	86.58	−0.0042 to −0.0043
	N7H···O2	4	0.040	0.097	11.30−11.32		−0.0058 to −0.0059
FdaX4·Na^+	N1H···O6	4	0.037	0.097−0.098	10.30−10.33	80.81	−0.0042 to −0.0043
	N7H···O2	4	0.036	0.091	9.88−9.89		−0.0043
FdaX4·K^+	N1H···O6	4	0.035−0.036	0.094−0.095	9.47−9.71	83.23	−0.0033 to −0.0036
	N7H···O2	4	0.040	0.096−0.097	11.17−11.29		−0.0058 to −0.0059
$(FdaX4)_2$	N1H···O6	8	0.041−0.043	0.104−0.108	11.84−12.49	163.92	−0.0055 to −0.0065
	N7H···O2	8	0.030−0.034	0.084−0.089	7.61−9.15		−0.0015 to −0.0034
$(FdaX4)_2$·Na^+	N1H···O6	8	0.042−0.044	0.102−0.104	11.90−12.69	187.20	−0.0062 to −0.0072
	N7H···O2	8	0.039−0.041	0.095−0.096	10.96−11.42		−0.0056 to −0.0062
$(FdaX4)_2$·K^+	N1H···O6	8	0.039−0.040	0.099−0.101	10.78−11.36	170.34	−0.0049 to −0.0055
	N7H···O2	8	0.037−0.038	0.093	10.02−10.37		−0.0045 to −0.0049
CldaX4	N1H···O6	4	0.037	0.098	10.32−10.36	84.67	−0.0042
	N7H···O2	4	0.039	0.097	10.82−10.83		−0.0052
CldaX4·Na^+	N1H···O6	4	0.038−0.039	0.099−0.100	10.76−10.78	81.60	−0.0047
	N7H···O2	4	0.036	0.092	9.64		−0.0039
CldaX4·K^+	N1H···O6	4	0.035	0.094	9.38−9.40	81.29	−0.0032
	N7H···O2	4	0.039	0.097	10.92−10.94		−0.0053 to −0.0054
$(CldaX4)_2$	N1H···O6	8	0.042−0.044	0.104−0.108	12.05−12.87	182.85	−0.0062 to −0.0071
	N7H···O2	8	0.036−0.039	0.093−0.096	9.96−10.84		−0.0042 to −0.0052
$(CldaX4)_2$·Na^+	N1H···O6	8	0.042−0.043	0.103−0.104	11.99−12.39	183.02	−0.0063 to −0.0066
	N7H···O2	8	0.038−0.039	0.094−0.095	10.54−10.94		−0.0050 to −0.0055
$(CldaX4)_2$·K^+	N1H···O6	8	0.040−0.041	0.102−0.103	11.46−11.63	167.27	−0.0054 to −0.0057
	N7H···O2	8	0.035	0.090−0.091	9.27−9.45		−0.0035 to −0.0037
$(X4)_2$·Na^{+f}	N1H···O6	8	0.042−0.044	0.102−0.105	11.89−12.64	174.77	−0.0065
	N7H···O2	8	0.034−0.036	0.089−0.092	9.15		−0.0038 to −0.0042
$(X4)_2$·K^{+f}	N1H···O6	8	0.038−0.040	0.099−0.101	10.64−11.45	157.07	−0.0046 to −0.0056
	N7H···O2	8	0.032−0.034	0.087−0.089	8.26−8.93		−0.0023 to −0.0031

[a]Number of times a particular H-bond occurs in a structure. [b]Ranges (from minimal to maximal values) for the electron density and the Laplacian of the electron density at the line critical point (LCP or (3,−1) critical point), atomic units. [c]Energy range (in kcal/mol) for H-bonds determined by the EML method (eq 5 in the Computational Methodology section). [d]Sum of all the NH···O H-bond energies E_{HB} (in kcal/mol) in a complex. [e]Total electron energy density at line critical point (3,−1), i.e. the sum of the potential energy density (virial field) and the kinetic electron energy density, atomic units. [f]Data from ref 46. [g]For comparison, the data for H-bonds in $(B4)_2$ models of unmodified xanthine (X) from ref 46 are also shown. The geometries were optimized in TURBOMOLE at the BLYP-D3/def2-TZVPP level of theory.[49] The wavefunctions for QTAIM analysis were obtained at the BLYP/def2-TZVPP level of theory in Gaussian 09.

Electron Deformation Density (EDD) and ETS-NOCV Analysis. Next, we used ETS-NOCV[57] methodology to provide insights into the electron density redistribution (electron deformation density, EDD) upon formation of the CldaX4 quartet (other 8-halo-9-deazaX tetrads were not considered since they have very similar geometric, energetic, and H-bonding properties with CldaX4). The same analysis was performed for guanine quartet G4, a natural reference used. The ETS-NOCV charge and energy decomposition scheme based on the Kohn−Sham approach makes it possible to arbitrarily select two (or more) bonded regions within a molecule or molecular complex and characterize shift of the electron density upon formation of the bond in terms of electron deformation density contributions, $\Delta\rho$ (eq 3 in Computational Methodology), and also provide quantitative energies, ΔE^k_{orb}, corresponding to each $\Delta\rho$ contribution (eq 4). The results are shown in Figure 5 and Figures S5 and S6 in the Supporting Information. The red and blue zones of electron deformation density (EDD) in Figure 5 (and Figures S5 and S6 in the Supporting Information) correspond to the regions of electron density reflux and influx, respectively, induced by formation of the quartet from two Hoogsteen base pairs.

In the G4 and CldaX4 tetrads the first four NOCV contributions ($\Delta\rho_1 + \Delta\rho_2 + \Delta\rho_3 + \Delta\rho_4$) represent formation of the four H-bonds, two N1H···O6 and two N7H···O2 (Figure 5 and Figures S5 and S6). Qualitatively, it is seen that these H-bonds involve charge transfer from the lone electron pair of oxygen atoms O6 or O2 to the empty σ^*(N1−H) or σ^*(N7−H) orbitals, respectively. In addition, one can notice some degree of charge depletion from the hydrogen atoms (covalency of H···O2 and H···O6 bonds). Quantitatively, the part of orbital-interaction stabilization responsible for these charge reorganizations is slightly more pronounced in the case of the G4 complex as compared to the CldaX4 tetrad, see Figure 5.

Quantum Theory of Atoms in Molecules (QTAIM) and EML Approach. To characterize H-bonds in terms of the electron density distribution and to estimate their energies, we performed topological analysis of the electron density in tetrads B4 and two-stack systems $(B4)_2$ based on Quantum Theory of Atoms in Molecules (QTAIM).[48] Table S5 in the Supporting Information displays the results of the topological analysis for H-bonds, van der Waals (vdW), and ion-base coordination contacts including the line critical point (LCP) characteristics as well as geometrical properties of each type of noncovalent interaction. The short summary of QTAIM analysis for H-bonds in 8-halo-9-deazaxanthine quadruplexes is presented in Table 3. The analysis of H-bond energy values (calculated by EML method, see eq 5) evidence that in $(B4)_2$·M^+ complexes which serve as first approximations to tetrad stem stacks in

dx.doi.org/10.1021/ct5007554 | J. Chem. Theory Comput. 2014, 10, 5353−5365

DNA quadruplexes, the aromatic $\pi-\pi$ stacking reinforces the internal N1H···O6 hydrogen bonds inside quartets compared to corresponding B4·M^+ tetrads (Table 3). This strengthening of N1H···O6 bonds upon stacking efficiently compensates its enfeebling due to Na^+/K^+ coordination to O6 atom in $(B4)_2\cdot M^+$. In general, the sum of all H-bonds energies in $(B4)_2\cdot M^+$ models exceeds the doubled sum of H-bond energies in corresponding B4 or B4·M^+ tetrads. For instance, for the $(FdaX4)_2\cdot Na^+$ model this sum is equal to 187.20 kcal/mol according to the EML[78] method, whereas the corresponding doubled sum for the FdaX4·Na^+ complex is 161.62 kcal/mol (Tables 3 and S5 in the Supporting Information). This difference can be in part assigned to the H-bond enhancement in the presence of aromatic $\pi-\pi$ stacking. It was found earlier[86] that stacking can increase the H-bonding ability of DNA bases. This effect was attributed[86] to the hardness and orientation of the stacking molecule: the softer the stacking molecule, the larger the charge transfer to the stacked one and thus the larger its ability of H-bonding. In addition, stacking was shown to inverse relative strengths of the two neighboring H-bonds in guanine-cytosine and guanine-methylcytosine base pairs.[87] In addition to the EML formula,[78] we also used the relationship for estimating H-bond energies suggested by Nikolaienko et al.[80] (Table S5 in the Supporting Information, energy values in brackets).

As far as LCP properties are concerned, the N1H···O6 and N7H···O2 H-bonds are characterized by rather high values of the electron density, ρ, and the Laplacian of the electron density, $\nabla^2\rho$ (Tables 3 and S5 in the Supporting Information). The positive sign of the $\nabla^2\rho$ suggests that H-bonds in the studied systems can be classified as closed-shell interactions.[48,88,89] However, the fact that the total energy density H (sum of the potential and kinetic energy densities) at the H-bond critical points (3,−1) is negative (Table 3) implies that H-bonds benefit from some degree of covalency.[90,91]

In addition to LCP characteristics, the QTAIM atomic properties of hydrogen atoms involved in H-bonding in Hoogsteen base pairs B2 and tetrads B4 (B = FdaX, CldaX) were analyzed. These properties included atomic charge q (H), dipolar polarization M (H), atomic energy E (H), and atomic volumes ν (H) and were compared for H-bonded and the reference H-bond-free states. In the latter case, the isolated FdaX and CldaX nucleobases were considered. For comparison purposes the same kind of analysis was also performed for dimers B2 and tetramers B4 of unmodified xanthine (X2 and X4) and natural guanine (G2 and G4). Based on these data, the following conclusions can be drawn: (i) The changes of atomic properties Δq, ΔM, $\Delta\nu$, and ΔE and their signs are in perfect agreement with Koch and Popelier criteria[92] of H-bonding; (ii) H-bonding in FdaX4 and CldaX4 tetrads affects hydrogen atoms properties more deeply relative to the xanthine tetrad, X4. In all cases the absolute values of Δq, ΔM, $\Delta\nu$, and ΔE are higher for FdaX4 and CldaX4 complexes than for the X4 one (Table S7 in the Supporting Information); (iii) When comparing the changes in atomic properties for base pairs B2 and tetrads B4, it can be seen (Table S7 in the Supporting Information) that the absolute values of Δq, ΔM, $\Delta\nu$, and ΔE substantially increase in tetramer G4 compared to dimer G2, whereas for xanthine and its 8-halo-9-deaza derivatives they can either increase or decrease in some cases. This fact serves as an additional evidence of strong H-bond cooperativity[13] in the G4 quartet.

Furthermore, QTAIM delocalization indices were calculated for each H-bond type in tetrads and two-stack systems (Table S8 in the Supporting Information). The delocalization index (DI) measures the degree of electron sharing, i.e., the covalency, between two atoms. The comparison of the DI values with corresponding H-bond energies calculated by means of EML formula (5) (Table S8 in the Supporting Information) suggests an excellent correlation between two quantities, the correlation coefficient being 0.97. The graphical representation of the correlation is shown in Figure 6.

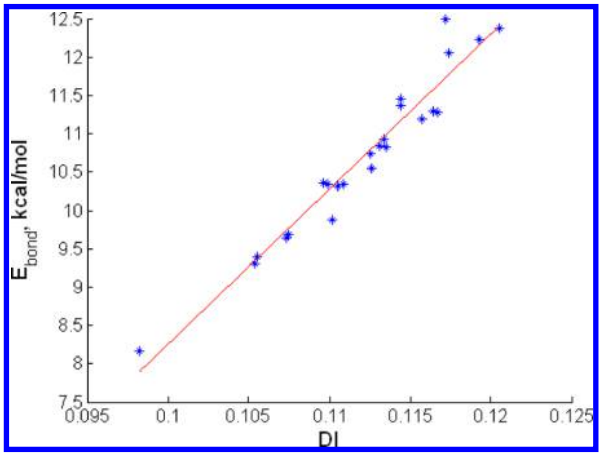

Figure 6. Graphical representation of relationship between delocalization indices (DI) and H-bonds energies (E_{bond}). The linear regression line is described by the formula E_{bond} [kcal/mol] = 202.3856*DI [au] − 11.9897. The mean square error is equal to 0.0667.

Therefore, our data point to an important role of a covalent component in controlling and tuning H-bond strengths in model DNA quadruplex structures: H-bonds get stronger as the degree of electron sharing between hydrogen and the acceptor (oxygen) atoms increases.

Finally, H-bonds were analyzed by NBO and compliance constants theory, which confirm the results of QTAIM analysis (see Tables S9 and S10 in the Supporting Information and comments to these tables).

3.4. Stacking. *Energy Decomposition Analysis.* To cast light on the interplay between forces that govern the tetrad stacking in our models, we applied energy decomposition analysis (EDA). First, two-stack systems without ions − $(FdaX4)_2$ and $(CldaX4)_2$ − were analyzed (Table 2). The stacking energy was estimated as interaction energy between two stacked tetrads, each representing a separate region. This energy amounts to −47.37 kcal/mol and −53.37 kcal/mol for $(FdaX4)_2$ and $(CldaX4)_2$ models, respectively. Thus, the suggested xanthine modifications lead to a considerable increase of quadruplex stability coming from the $\pi-\pi$ stacking. For comparison purposes, the corresponding stacking energies in $(X4)_2$ and $(G4)_2$ models are −42.02 kcal/mol and −33.76 kcal/mol, respectively.[46] The analysis of individual contributions (Table 2) to the interaction energy, ΔE_{int}, demonstrates that the dispersion part (−72.56 kcal/mol in $(FdaX4)_2$ and −82.22 kcal/mol in $(CldaX4)_2$) makes the crucial contribution to the stacking although electrostatic, ΔV_{elstat}, and orbital interaction, ΔE_{oi}, terms also play important roles in stabilizing the tetrad stacks. In three-stack models $(FdaX4)_3$ and $(CldaX4)_3$ the interaction energies between quartet layers are −98.02 kcal/mol and −111.03 kcal/mol, respectively, which

dx.doi.org/10.1021/ct5007554 | J. Chem. Theory Comput. 2014, 10, 5353−5365

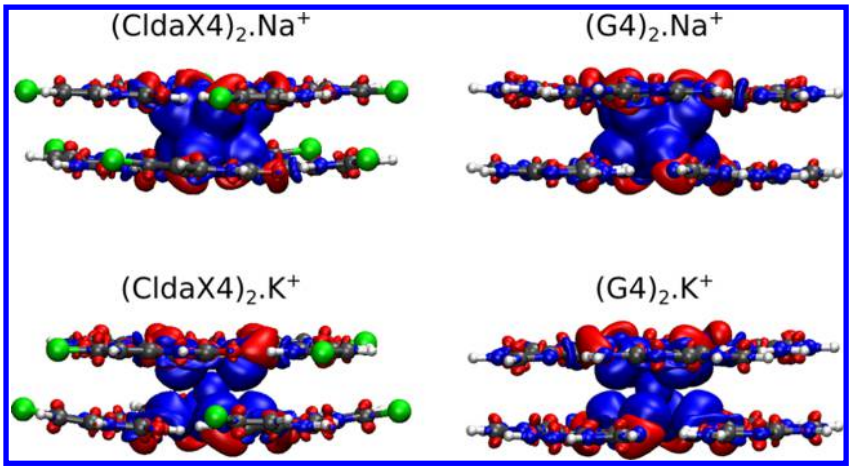

Figure 7. Electron deformation density (EDD) showing charge concentration around O6 atoms and charge influx to the Na^+ (top) or K^+ (bottom) ion upon its coordination to the system of two stacked CldaX (left) and G (right) tetrads (for the top views, see Figure S7). The contour values are ±0.0005 au.

somewhat exceeds the doubled stacking energies in $(FdaX4)_2$ and $(CldaX4)_3$, i.e. −94.74 kcal and −106.74 kcal/mol. This fact can be assigned to the phenomenon of a weak cooperativity in stacking, which was also detected in xanthine-containing model DNA quadruplex structures.[46] In addition, analysis of three-stack systems $(BrdaX4)_3$ and $(IdaX4)_3$ provides evidence that the presence of heavier halogen atom at position 8 (Br or I) leads to further increase in the stabilization coming from $\pi-\pi$ stacking (ΔE_{int} is equal to −117.55 kcal/mol and −120.78 kcal/mol for $(BrdaX4)_3$ and $(IdaX4)_3$ systems, respectively). It is noteworthy that this increase is controlled mainly by the dispersion, ΔE_{disp}, and electrostatic term, ΔV_{elstat}, involving also non-neighboring tetrads. To sum up, EDA approach corroborates the efficiency of the described xanthine modifications in enhancing stability of tetrad stacks in quadruplex DNA.

Noncovalent Interaction Plots. We also carried out the NCI plot analysis to elucidate some features of the tetrad stacking in FdaX- and CldaX-based model DNA quadruplex structures (see Figure 4 and Figure S3 in the Supporting Information). As expected, the areas of the stacking iso-surfaces in the $(FdaX4)_2{\cdot}Na^+$ and $(CldaX4)_2{\cdot}Na^+$ systems were found to be larger than in the corresponding two-stack complex of unmodified xanthine,[46] $(X4)_2{\cdot}Na^+$ (see Figures S3 and S4 and comments to Figure S4 in the Supporting Information). The mutual interplay of H-bonding and stacking can serve as a possible explanation. It was shown earlier that neighboring H-bonds in intermolecular complexes are capable of forming pseudoaromatic rings,[93,94] which participate in stacking. The effect of stacking between pseudoaromatic rings is directly connected with the strength of H-bonds forming these rings. Therefore, we assume that stronger H-bonds in tetrads of $(FdaX4)_2{\cdot}Na^+$ and $(CldaX4)_2{\cdot}Na^+$ models lead to the formation of stronger pseudoaromatic rings as compared to $(X4)_2{\cdot}Na^+$ and, consequently, contribute to more favorable stacking between them.

3.5. Ion Coordination. *Energy Decomposition Analysis.* First, the Na^+/K^+ binding to the model DNA quadruplex structures was elucidated with the help of the energy decomposition analysis (EDA). We started with the simplest models − $B4{\cdot}M^+$ optimized complexes, where the M^+ ion represents one interacting region, and the rest of the system (tetrad) the other one. The results (Table 2) indicate that the Na^+ ion tends to bind to tetrads more strongly than the K^+ ion. The scrutiny of the individual terms contributing to the Na^+/K^+ coordination to tetrads gives evidence for a dominant role of the electrostatic part (ΔV_{elstat}) in this stabilizing interaction. However, the orbital term, ΔE_{oi}, accounting for the charge transfer and polarization makes up to ∼50% of the ΔV_{elstat} contribution and, therefore, cannot be neglected. Similarly to tetrads, in two-stack and three-stack systems the prevailing contribution to the stabilization comes from the electrostatic term, ΔV_{elstat}, with a noticeable supplement from the orbital part, ΔE_{oi}. Finally, we estimated the energy of the interaction of the ion with $(FdaX4)_3{\cdot}M^+$ or $(CldaX4)_3{\cdot}M^+$ system containing another ion of the same type inside the pore (Table 2). As expected, the availability of another ion inside the channel reduces the interaction energy of the second ion with the rest of the system due to electrostatic repulsion between the ions (Table 2). Analysis of ion coordination in the $(BrdaX4)_3{\cdot}2Na^+$ and $(IdaX4)_3{\cdot}2Na^+$ complexes shows that the interaction energy of the Na^+ ion with the rest of the systems is slightly increased as compared to corresponding FdaX- and CldaX-containing systems, and this additional stabilization comes from the change in the electrostatic term, ΔV_{elstat}.

The EDA analysis of Na^+/K^+ coordination in tetrads, two- and three-stack systems shows that (i) The Na^+ ion tends to coordinate more strongly than K^+ (however, ion desolvation is neglected). This can be explained by the smaller ionic radius of Na^+ compared to K^+ and, therefore, less pronounced steric effect, which is reflected in the exchange-repulsion term, ΔE_{ex} (Table 2); (ii) The suggested xanthine modifications increase the ion-binding affinity of model quadruplexes: in all the B4, $(B4)_2$, and $(B4)_3$ models containing 8-halo-9-deazaxanthines the Na^+/K^+ interaction energy is higher relative to the corresponding X complexes.[46]

Despite the dominant role of the electrostatic forces (expressed by the ΔV_{elstat} contribution) in the total interaction energy, ΔE_{int}, the Na^+/K^+ coordination might not be considered as purely electrostatic. There is rather noticeable input of the orbital term, ΔE_{oi}, which is partially balanced by the exchange-repulsion term, ΔE_{ex}. In a nutshell, the difference between Na^+ and K^+ binding (in vacuo) originates in the exchange-repulsion term, whereas the differences between individual halogenated derivatives come from the electrostatic term (see Table 2).

dx.doi.org/10.1021/ct5007554 | J. Chem. Theory Comput. 2014, 10, 5353−5365

Electron Deformation Density and ETS-NOCV Analysis. To investigate the electron redistribution upon the ion binding to $(B4)_2$, we calculated the electron deformation density for the $(B4)_2{\cdot}M^+$ systems. Figure 7 shows the total EDD, $\Delta\rho$, for the interaction of Na^+ (top) or K^+ (bottom) with CldaX (left) or G (right) systems (for a top view, see Figure S7 in the Supporting Information); the red regions of deformation density ($\Delta\rho < 0$) are located on the lower and upper quartets, whereas the blue areas ($\Delta\rho > 0$) are concentrated in the vicinity of the M^+ showing the influx of electron density from the systems of two stacked tetrads to the M^+.

In addition, ETS-NOCV methodology was applied to figure out the main contributions to the EDD and monitor details of electron redistribution. In the course of the ETS-NOCV decomposition scheme two representative structures – $(CldaX4)_2{\cdot}Na^+$ and $(CldaX4)_2{\cdot}K^+$ – were considered. The first three NOCV contributions for the $(CldaX4)_2{\cdot}Na^+$ system correspond to the electron density influx via different channels to the M^+ (for individual NOCV pair contributions and their energies as well as their sum, see Figures S8–S10 in the Supporting Information). It should be highlighted that the first channel corresponds to the electron density influx from all eight oxygen atoms toward the Na^+ (E^1_{orb} = −4.37 kcal/mol; $\Delta\rho_1$ for $(CldaX4)_2{\cdot}Na^+$ in Figure 8). In contrast, an analogous channel

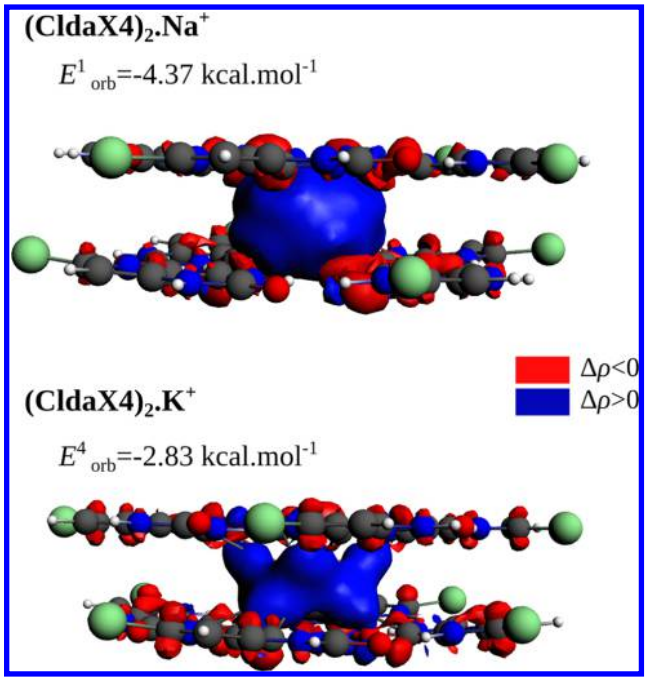

Figure 8. Contributions to electron deformation density (EDD) showing charge influx to the Na^+ (top, $\Delta\rho_1$) or K^+ (bottom, $\Delta\rho_4$) upon its coordination to the $(CldaX4)_2$ system (for eight most important channels, see Figures S8–13). The contour values are ±0.0001 au.

for the $(CldaX4)_2{\cdot}K^+$ system contributes notably less to the stability of the complex (E^4_{orb} = −2.83 kcal/mol; $\Delta\rho_4$ for $(CldaX4)_2{\cdot}K^+$ in Figure 8 and Figures S11–13 in the Supporting Information). The above-mentioned differences indicate that Na^+ induces a larger polarization of electron density in quadruplex toward the ion as compared with K^+. To support this observation by additional approaches we performed VDD and QTAIM analyses.

Voronoi Deformation Density (VDD) and QTAIM Delocalization Index. Taking into account the above-mentioned role of the polarization or charge transfer, we analyzed the values of the Voronoi deformation density (VDD) charges on Na^+/K^+ upon their coordination to the quadruplex systems (Table 2). The physical meaning of VDD charge, Q_A, associated with an atom A, is the following: it serves as a measure of the charge flow, due to chemical interaction, out of ($Q_A > 0$) or into ($Q_A < 0$) the Voronoi cell of atom A, that is, the region of space that is closer to nucleus A than to any other nucleus.[95] The obtained values of VDD charges for Na^+/K^+ ions are negative, which points out to the direction of the electron density flow upon metal cation coordination (from quadruplex to Na^+/K^+). It should be also noted that in all cases the Na^+ ion bears more negative VDD charge (−0.085 to −0.080 for different models) than K^+ (−0.062 to −0.057).

The values of QTAIM delocalization indices (DI) for O6···Na^+ and O6···K^+ contacts in $(B4)_2{\cdot}M^+$ fall into the 0.030–0.048 and 0.064–0.071 au ranges, respectively (Table S8 in the Supporting Information). Although DI values for ion-base coordination contacts are smaller than those for N1H···O6 and N7H···O2 hydrogen bonds, they are commensurable (i.e., of the same order of magnitude) in both cases. This fact indicates some role of the electron sharing in Na^+/K^+ coordination inside the quadruplex channel which is more important for K^+.

To conclude, the analysis of electron deformation density and QTAIM delocalization indices suggests that the larger electron polarization from the quadruplex toward the ion is induced by Na^+ as compared to K^+, whereas K^+ has a higher propensity to electron sharing. However, the possible impact of the polarization/charge transfer on the ion dynamics within the quadruplex channel[45−47,96] should be verified and tested by other approaches, which is beyond the scope of this study.

4. CONCLUDING REMARKS

Nowadays, nucleic acids are finding applications in various areas of bio- and nanotechnology. In this regard, it is quite important to develop efficient strategies that allow probing the DNA quadruplex core via chemical modifications to further enhance their stability and specific properties. One of the computational strategies has been suggested in our recent work.[47] In the present paper we analyze systematically the energetics, structural features, and especially noncovalent interactions in model nucleic acid quadruplexes incorporating 8-halo-9-deazaxanthine nucleobases (containing F, Cl, Br, or I). By applying modern state-of-the-art computational techniques – DFT-D3 calculations, QTAIM and NBO analyses, Grunenberg's compliance constant theory, energy decomposition schemes such as EDA and ETS-NOCV, Voronoi deformation density (VDD) charges – we reveal distinctive features of halogen-containing models through their comparison with the corresponding xanthine (X) and guanine (G) structures.

It is found that the proposed X modifications perceptibly enhance the stability of the DNA quadruplex core. By means of EDA and QTAIM/EML analysis it is established that the energies of individual H-bonds in halogen-containing complexes slightly increase compared to the reference X-containing structures.[46] Quadruplex systems incorporating polarizable halogen atoms benefit significantly from the stabilizing stacking between the individual tetrads due to an increased dispersion contribution as compared to xanthine, a natural reference used. However, further *in silico* design of artificial quadruplexes with

dx.doi.org/10.1021/ct5007554 | J. Chem. Theory Comput. 2014, 10, 5353−5365

Br- or I-containing nucleobases is hampered by unfeasibility to model these structures by means of standard explicit solvent MD simulations. The other potential issue in using BrdaX and IdaX units for constructing the DNA quadruplexes consists in assumed lower stability of C−Br and C−I covalent bonds (compared to C−F and C−Cl ones), which may result in their cleavage under certain conditions. This issue must be explored experimentally.

As far as the ion coordination is concerned, its analysis by various methods suggests that, despite the dominating electrostatic contribution, it cannot be considered as purely electrostatic and is influenced by significant electron redistribution. This fact is evidenced by the energy decomposition analysis, the QTAIM delocalization index, and by visualizing the electron deformation density (analyzed using ETS-NOCV), which demonstrates the significant charge density influx in the region of the monovalent ion. Accounting for the effect of this electron redistribution in molecular dynamics simulations would require a careful parametrization of the force field. We expect that our results will contribute to the development of novel strategies to further modify and analyze the quadruplex DNA core.

■ ASSOCIATED CONTENT

Ⓢ Supporting Information

Computational details, additional figures with optimized DNA quadruplex models, NCI surfaces for xanthine (X) and 8-fluoro-9-deaza-xanthine-containing structures, reduced density gradient vs $sign(\lambda_2)\rho$ plots for $(B4)_2{\cdot}Na^+$ models, contours with individual NOCV deformation density contributions for H-bonding and ion coordination, tables with van der Waals volumes of model quadruplexes, formation energies, characteristics of planar structures, values of the twist angle, detailed results of QTAIM analysis, additional energy decomposition analysis for selected structures optimized at the BLYP-D3/TZP level of theory, "two-molecules" characteristics of H-bonds, H-bond delocalization indices, NBO analysis, compliance constants and NPA charges for H-bonds and van der Waals interactions. This material is available free of charge via the Internet at http://pubs.acs.org.

■ AUTHOR INFORMATION

Corresponding Author

*E-mail: rmarek@chemi.muni.cz.

Notes

The authors declare no competing financial interest.

■ ACKNOWLEDGMENTS

Y.P.Y. is deeply grateful to Dr. Tymofii Nikolaienko (Kiev National University) for helpful discussions. This work was carried out at CEITEC − the Central European Institute of Technology with research infrastructure supported by the project CZ.1.05/1.1.00/02.0068 financed by the European Regional Development Fund and in project INBIOR (CZ.1.07/2.3.00/20.0042) from the European Social Fund and the state budget of the Czech Republic. The access to the CERIT-SC computing and storage facilities provided under the program Center CERIT Scientific Cloud, part of the Operational Program Research and Development for Innovations (CZ.1.05/3.2.00/08.0144), is highly appreciated.

■ REFERENCES

(1) Neidle, S. *Principles of nucleic acid structure*; Elsevier: Amsterdam, 2008.
(2) Blackburn, E. H. *Nature* **1991**, *350*, 569.
(3) Neidle, S.; Parkinson, G. *Nat. Rev. Drug Discovery* **2002**, *1*, 383.
(4) Grand, C. L.; Han, H.; Muñoz, R. M.; Weitman, S.; Von Hoff, D. D.; Hurley, L. H.; Bearss, D. J. *Mol. Cancer Ther.* **2002**, *1*, 565.
(5) Sun, H.; Yabuki, A.; Maizels, N. *Proc. Natl. Acad. Sci. U. S. A.* **2001**, *98*, 12444.
(6) Wen, J. D.; Gray, C. W.; Gray, D. M. *Biochemistry* **2001**, *40*, 9300.
(7) Mohaghegh, P.; Karow, J. K.; Brosh, R. M.; Bohr, V. A.; Hickson, I. D. *Nucleic Acids Res.* **2001**, *29*, 2843.
(8) Biffi, G.; Tannahill, D.; McCafferty, J.; Balasubramanian, S. *Nat. Chem.* **2013**, *5*, 182.
(9) Hobza, P.; Müller-Dethlefs, K. *Non-covalent interactions: Theory and Experiment* (RSC Theoretical and Computational Chemistry Series No. 2), RSC Publishing: Cambridge, 2010.
(10) van Mourik, T.; Dingley, A. J. *Chem.—Eur. J.* **2005**, *11*, 6064.
(11) Louit, G.; Hocquet, A.; Ghomi, M.; Meyer, M.; Sühnel, J. *PhysChemComm* **2003**, *6*, 1.
(12) Louit, G.; Hocquet, A.; Ghomi, M.; Meyer, M.; Sühnel, J. *PhysChemComm* **2002**, *5*, 94.
(13) Fonseca Guerra, C.; Zijlstra, H.; Paragi, G.; Bickelhaupt, M. *Chem.—Eur. J.* **2011**, *17*, 12612.
(14) Jissy, A. K.; Ashik, U. P. M.; Datta, A. *J. Phys. Chem. C* **2011**, *115*, 12530.
(15) Gu, J.; Leszczynski, J. *J. Phys. Chem. A* **2000**, *104*, 6308.
(16) Meyer, M.; Brandl, M.; Sühnel, J. *J. Phys. Chem. A* **2001**, *105*, 8223.
(17) Meyer, M.; Sühnel, J. *J. Biomol. Struct. Dyn.* **2003**, *20*, 507.
(18) Clay, E. H.; Gould, I. R. *J. Mol. Graphics Modell.* **2005**, *24*, 138.
(19) Lech, C. J.; Heddi, B.; Phan, A. T. *Nucleic Acids Res.* **2013**, *41*, 2034.
(20) Šponer, J.; Mládek, A.; Špačková, N.; Cheatham, T. E., 3rd; Grimme, S. *J. Am. Chem. Soc.* **2013**, *135*, 9785.
(21) Liu, H.; Gauld, J. W. *Phys. Chem. Chem. Phys.* **2009**, *11*, 278.
(22) Ilchenko, M. M.; Dubey, I. Ya. *Int. Rev. Biophys. Chem.* **2011**, *2*, 82.
(23) Deepa, P.; Kolandaivel, P.; Senthilkumar, K. *Comput. Theor. Chem.* **2011**, *974*, 57.
(24) Meng, F.; Xu, W.; Liu, C. *Chem. Phys. Lett.* **2004**, *389*, 421.
(25) Gu, J.; Leszczynski, J.; Bansal, M. *Chem. Phys. Lett.* **1999**, *311*, 209.
(26) Haider, S.; Neidle, S. *Methods Mol. Biol.* **2010**, *608*, 17.
(27) Šponer, J.; Cang, X.; Cheatham, T. E., 3rd *Methods* **2012**, *57*, 25.
(28) Akhshi, P.; Gregory, A.; Wu, G. *J. Phys. Chem. B* **2012**, *116*, 9363.
(29) Agrawal, S.; Ojha, R. P.; Maiti, S. *J. Phys. Chem. B* **2008**, *112*, 6828.
(30) Cang, X.; Šponer, J.; Cheatham, T. E., 3rd *J. Am. Chem. Soc.* **2011**, *133*, 14270.
(31) Davis, J. T. *Angew. Chem., Int. Ed.* **2004**, *43*, 668.
(32) Niemeyer, C. M.; Adler, M. *Angew. Chem., Int. Ed.* **2002**, *114*, 3779.
(33) Delaney, S.; Barton, J. K. *Biochemistry* **2003**, *42*, 14159.
(34) Marsh, T. C.; Henderson, E. *Biochemistry* **1994**, *33*, 10.718.
(35) Abu-Ghazalah, R. M.; Irizar, J.; Helmy, A. S.; Macgregor, R. B., Jr. *Biophys. Chem.* **2010**, *147*, 123.
(36) Mendez, M. A.; Szalai, V. A. *Nanoscale Res. Lett.* **2013**, *8*, 210.
(37) Yatsunyk, L. A.; Piétrement, O.; Albrecht, D.; Tran, P. L. T.; Renčiuk, D.; Sugiyama, H.; Arbona, J.-M.; Aimé, J.-P.; Mergny, J.-L. *ACS Nano* **2013**, *7*, 5701.
(38) Kaucher, M. S.; Harrell, W. A.; Davis, J. T. *J. Am. Chem. Soc.* **2006**, *128*, 38.
(39) Hud, N.; Schultze, P.; Sklenar, V.; Feigon, J. *J. Mol. Biol.* **1999**, *285*, 233.
(40) Shi, X. D.; Fettinger, J. C.; Cai, M. M.; Davis, J. T. *Angew. Chem., Int. Ed.* **2000**, *39*, 3124.

(41) van der Wijst, T.; Fonseca Guerra, C.; Swart, M.; Bickelhaupt, M.; Lippert, B. *Angew. Chem., Int. Ed.* **2009**, *48*, 3285.
(42) Paragi, G.; Kovács, L.; Kupihár, Z.; Szolomájer, J.; Penke, B.; Fonseca Guerra, C.; Bickelhaupt, F. M. *New. J. Chem.* **2011**, *35*, 119.
(43) Szolomájer, J.; Paragi, G.; Batta, G.; Fonseca Guerra, C.; Bickelhaupt, F. M.; Kele, Z.; Pádár, P.; Kupihár, Z.; Kovács, L. *New. J. Chem.* **2011**, *35*, 476.
(44) Ciesielski, A.; Haar, S.; Bényei, A.; Paragi, G.; Fonseca Guerra, C.; Bickelhaupt, F. M.; Masiero, S.; Szolomájer, J.; Samori, P.; Spada, G. P.; Kovács, L. *Langmuir* **2013**, *29*, 7283.
(45) Novotný, J.; Kulhánek, P.; Marek, R. *J. Phys. Chem. Lett.* **2012**, *3*, 1788.
(46) Yurenko, Y. P.; Novotný, J.; Sklenář, V.; Marek, R. *Phys. Chem. Chem. Phys.* **2014**, *16*, 2072.
(47) Novotný, J.; Yurenko, Y. P.; Kulhánek, P.; Marek, R. *Phys. Chem. Chem. Phys.* **2014**, *16*, 15241.
(48) Bader, R. F. W. *Atoms in Molecules: A Quantum theory*; Oxford University Press: New York, US, 1990.
(49) Weinhold, F.; Landis, C. R. *Valency and Bonding. A Natural Bond Orbital Donor-Acceptor Perspective*; Cambridge University Press: UK, 2005.
(50) Brandhorst, K.; Grunenberg, J. *Chem. Soc. Rev.* **2008**, *37*, 1558.
(51) Brandhorst, K.; Grunenberg, J. *J. Chem. Phys.* **2010**, *132*, 184101.
(52) Grunenberg, J.; Barone, G. *RSC Adv.* **2013**, *3*, 4757.
(53) Brandhorst, K.; Grunenberg, J. *ChemPhysChem* **2007**, *8*, 1151.
(54) Grunenberg, J. *Phys. Chem. Chem. Phys.* **2011**, *13*, 10136.
(55) Kitaura, K.; Morokuma, K. *Int. J. Quantum Chem.* **1976**, *10*, 325−340.
(56) te Velde, G.; Bickelhaupt, F. M.; Baerends, E. J.; Fonseca Guerra, C.; van Gisbergen, S. J. A.; Snijders, J. G.; Ziegler, T. *J. Comput. Chem.* **2001**, *22*, 931.
(57) Mitoraj, M. P.; Michalak, A.; Ziegler, T. *J. Chem. Theory Comput.* **2009**, *5*, 962.
(58) Dyduch, K.; Mitoraj, M. P.; Michalak, A. *J. Mol. Model.* **2013**, *19*, 2747.
(59) Johnson, E. R.; Keinan, S.; Mori-Sanchez, P.; Contreras-Garcia, J.; Cohen, A. J.; Yang, W. *J. Am. Chem. Soc.* **2010**, *132*, 6498.
(60) Contreras-Garcia, J.; Johnson, E. R.; Keinan, S.; Chaudret, R.; Piquemal, J.-P.; Beratan, D. N.; Wang, W. *J. Chem. Theory Comput.* **2011**, *7*, 625.
(61) Sagi, J. *J. Biomol. Struct. Dyn.* **2014**, *32*, 477−511.
(62) Klamt, A.; Schüürmann, G. *J. Chem. Soc., Perkin Trans.* **1993**, *2*, 799.
(63) TURBOMOLE V6.3 2011, a development of University of Karlsruhe and Forschungzentrum Karlsruhe GmbH, 1989−2007, TURBOMOLE GmbH, since 2007. Available from http://www.turbomole.com (accessed Sept 10, 2014).
(64) Becke, A. D. *Phys. Rev.* **1988**, *38*, 3098.
(65) Lee, C.; Yang, W.; Parr, R. G. *Phys. Rev. B* **1988**, *37*, 785.
(66) Grimme, S.; Antony, J.; Ehrlich, S.; Krieg, H. *J. Chem. Phys.* **2010**, *132*, 154104.
(67) Jurečka, P.; Šponer, J.; Černý, J.; Hobza, P. *Phys. Chem. Chem. Phys.* **2006**, *8*, 1985.
(68) Riley, K. E.; Vondrášek, J.; Hobza, P. *Phys. Chem. Chem. Phys.* **2007**, *9*, 5555.
(69) ADF2012.01, SCM, *Theoretical Chemistry*; Vrije Universiteit: Amsterdam, The Netherlands, http://www.scm.com (accessed Sept 10, 2014).
(70) Ziegler, T.; Rauk, A. *Inorg. Chem.* **1979**, *18*, 1755.
(71) Nalewajski, R. F.; Mrozek, J.; Michalak, A. *Int. J. Quantum Chem.* **1997**, *61*, 589.
(72) Keith, T. A. *AIMAll* (Version 12.09.23, Professional), 2012. Retrieved from http://www.aim.tkgristmill.com (accessed Sept 10, 2014).
(73) Foroutan-Nejad, C.; Shahbazian, S.; Marek, R. *Chem.—Eur. J.* **2014**, *20*, 10140.
(74) Frisch, M. J.; Trucks, G. W.; Schlegel, H. B.; Scuseria, G. E.; Robb, M. A.; Cheeseman, J. R.; Scalmani, G.; Barone, V.; Mennucci, B.; Petersson, G. A.; Nakatsuji, H.; Caricato, M.; Li, X.; Hratchian, H. P.; Izmaylov, A. F.; Bloino, J.; Zheng, G.; Sonnenberg, J. L.; Hada, M.; Ehara, M.; Toyota, K.; Fukuda, R.; Hasegawa, J.; Ishida, M.; Nakajima, T.; Honda, Y.; Kitao, O.; Nakai, H.; Vreven, T.; Montgomery, J. A., Jr.; Peralta, J. E.; Ogliaro, F.; Bearpark, M.; Heyd, J. J.; Brothers, E.; Kudin, K. N.; Staroverov, V. N.; Keith, T.; Kobayashi, R.; Normand, J.; Raghavachari, K.; Rendell, A.; Burant, J. C.; Iyengar, S. S.; Tomasi, J.; Cossi, M.; Rega, N.; Millam, J. M.; Klene, M.; Knox, J. E.; Cross, J. B.; Bakken, V.; Adamo, C.; Jaramillo, J.; Gomperts, R.; Stratmann, R. E.; Yazyev, O.; Austin, A. J.; Cammi, R.; Pomelli, C.; Ochterski, J. W.; Martin, R. L.; Morokuma, K.; Zakrzewski, V. G.; Voth, G. A.; Salvador, P.; Dannenberg, J. J.; Dapprich, S.; Daniels, A. D.; Farkas, O.; Foresman, J. B.; Ortiz, J. V. ; Cioslowski, J.; Fox, D. J. *Gaussian 09*; Gaussian, Inc.: Wallingford, CT, 2010.
(75) Weigend, F.; Ahlrichs, R. *Phys. Chem. Chem. Phys.* **2005**, *7*, 3297.
(76) Feller, D. *J. Comput. Chem.* **1996**, *17*, 1571.
(77) Schuchardt, K. L.; Didier, B. T.; Elsethagen, T.; Sun, L.; Gurumoorthi, V.; Chase, J.; Li, J.; Windus, T. L. *J. Chem. Inf. Model.* **2007**, *47*, 1045.
(78) Espinosa, E.; Molins, E.; Lecomte, C. *Chem. Phys. Lett.* **1998**, *285*, 170.
(79) Mata, I.; Alkorta, I.; Espinosa, E.; Molins, E. *Chem. Phys. Lett.* **2011**, *507*, 185.
(80) Nikolaienko, T. Y.; Bulavin, L. A.; Hovorun, D. M. *Phys. Chem. Chem. Phys.* **2012**, *14*, 7441.
(81) Grunenberg, J. *J. Am. Chem. Soc.* **2004**, *126*, 16310.
(82) Ponomareva, A. G.; Yurenko, Y. P.; Zhurakivsky, R. O.; Van Mourik, T.; Hovorun, D. M. *J. Biomol. Struct. Dyn.* **2014**, *32*, 730.
(83) Ponomareva, A. G.; Yurenko, Y. P.; Zhurakivsky, R. O.; Van Mourik, T.; Hovorun, D. M. *Phys. Chem. Chem. Phys.* **2012**, *14*, 6787.
(84) Pedretti, A.; Villa, L.; Vistoli, G. *J. Mol. Graphics* **2002**, *21*, 47.
(85) Šponer, J.; Šponer, J. E.; Mládek, A.; Jurečka, P.; Banáš, P.; Otyepka, M. *Biopolymers* **2013**, *99*, 978.
(86) Mignon, P.; Loverix, S.; Steyaert, J.; Geerlings, P. *Nucleic Acids Res.* **2005**, *33*, 1779.
(87) Acosta-Silva, C.; Branchadell, V.; Bertran, J.; Oliva, A. *J. Phys. Chem. B* **2010**, *114*, 10217.
(88) Matta, C. F.; Castillo, N.; Boyd, R. J. *J. Phys. Chem. B* **2006**, *110*, 563.
(89) Matta, C. F.; Castillo, N.; Boyd, R. J. *J. Phys. Chem. A* **2005**, *109*, 3669.
(90) Jenkins, S.; Morrison, I. *Chem. Phys. Lett.* **2000**, *317*, 97.
(91) Grabowski, S. J. *Chem. Rev.* **2011**, *111*, 2597.
(92) Koch, U.; Popelier, P. L. A. *J. Phys. Chem.* **1995**, *99*, 9747.
(93) Dannenberg, J. J.; Rios, R. *J. Phys. Chem.* **1994**, *98*, 6714.
(94) Dutta, A.; Jana, A. D.; Gangopadhyay, S.; Das, K. K.; Marek, J.; Marek, R.; Brus, J.; Ali, M. *Phys. Chem. Chem. Phys.* **2011**, *13*, 15845.
(95) Fonseca Guerra, C.; Handgraaf, J. W.; Baerends, E. J.; Bickelhaupt, F. M. *J. Comput. Chem.* **2004**, *25*, 189.
(96) Gkionis, K.; Kruse, H.; Platts, J. A.; Mládek, A.; Koča, J.; Šponer, J. *J. Chem. Theory Comput.* **2014**, *10*, 1326.
(97) van Lenthe, E.; Ehlers, A. E.; Baerends, E. J. *J. Chem. Phys.* **1999**, *110*, 8943.